nature neuroscience

An astrocyte-dependent mechanism for neuronal rhythmogenesis

Philippe Morquette[1], Dorly Verdier[1], Aklesso Kadala[1], James Féthière[2], Antony G Philippe[3,4], Richard Robitaille[1] & Arlette Kolta[1,5]

Communication between neurons rests on their capacity to change their firing pattern to encode different messages. For several vital functions, such as respiration and mastication, neurons need to generate a rhythmic firing pattern. Here we show in the rat trigeminal sensori-motor circuit for mastication that this ability depends on regulation of the extracellular Ca^{2+} concentration ($[Ca^{2+}]_e$) by astrocytes. In this circuit, astrocytes respond to sensory stimuli that induce neuronal rhythmic activity, and their blockade with a Ca^{2+} chelator prevents neurons from generating a rhythmic bursting pattern. This ability is restored by adding S100β, an astrocytic Ca^{2+}-binding protein, to the extracellular space, while application of an anti-S100β antibody prevents generation of rhythmic activity. These results indicate that astrocytes regulate a fundamental neuronal property: the capacity to change firing pattern. These findings may have broad implications for many other neural networks whose functions depend on the generation of rhythmic activity.

The pattern of activity that emerges from a neuronal network defines the essence of its function. Many fundamental nervous functions, including attention, learning and memory, and control of sleep/wake cycle, result from rhythmic or oscillatory activities in neuronal networks. Obvious examples of such functions are rhythmic movements such as walking, breathing and chewing, which are generated by networks referred to as central pattern generators (CPGs)[1–3]. These networks generate a rhythmic motor activity that is continuously adjusted by sensory feedback to produce a movement pattern that is adapted to the prevailing conditions. Despite intense research in this field, the exact mechanisms underlying generation of this rhythmic activity and its adaptation by sensory inputs remain elusive. Some studies point to intrinsic pacemaker properties, while others emphasize synaptic connections[4]. In a few models, rhythmic network properties emerge from the combination of intrinsic properties and synaptic connections, but the mechanism underlying their interaction is ill-defined[5]. In most instances, the potential contribution of astrocytes, the most abundant type of cell in the brain, is largely ignored. Only in respiration has it been shown that astrocytes contribute, by detecting pH changes in the blood and modulating neuronal firing in response[6,7].

Several ionic conductances endow neurons with rhythmogenic abilities. I_{NaP}, a persistent voltage-dependent sodium current, is one such conductance that has been shown to underlie rhythmogenesis in the cortex, the hippocampus and several brainstem and spinal CPG systems. Rhythmogenic neurons of the trigeminal circuit involved in mastication and of the spinal locomotor CPG have I_{NaP}-mediated rhythmic bursting properties that are enhanced when the extracellular Ca^{2+} concentration ($[Ca^{2+}]_e$) diminishes[8,9]. Here we propose that this Ca^{2+} dependency forms the basis of the mechanism that enables synaptic inputs of sensory afferents to interact with intrinsic bursting properties and determines the neuronal ability to change firing pattern. We found that, in the dorsal part of the trigeminal main sensory nucleus (NVsnpr), where rhythmogenic neurons are found, stimulation of sensory fibers that project to the nucleus activated astrocytes. In turn, astrocytes regulated the external Ca^{2+} to trigger bursting by releasing a Ca^{2+} binding protein, S100β. Specific inactivation of astrocytes prevented neuronal bursting, which could be rescued only by addition of S100β; conversely, bursting could not be produced when S100β was blocked. These results will help understand the mechanisms leading to rhythmic firing and may have widespread implications for normal functions relying on rhythmogenesis, as well as abnormal rhythmic firing observed in several pathologies, such as Parkinson disease or epilepsy, where astrocytes are known to contribute.

RESULTS

Burst-inducing stimuli decrease external calcium

We showed in previous work that rhythmic bursting could be elicited in NVsnpr neurons by artificially reducing the Ca^{2+} concentration of the perfusing medium[9]. Decreases of $[Ca^{2+}]_e$ have been reported to occur during intense or sustained neuronal activity[10] or during pharmacologically induced locomotor-like activities in isolated neonatal rodent spinal cords[11], but it is unknown whether they occur in

[1]Département de Neurosciences and Groupe de Recherche sur le Système Nerveux Central, Université de Montréal, Montréal, Québec, Canada. [2]Faculté de Pharmacie, Université de Montréal, Montréal, Québec, Canada. [3]Faculté des Sciences du Sport, Université Montpellier 1, Montpellier, France. [4]Institut National de la Recherche Agronomique, UMR866 Dynamique Musculaire Et Métabolisme, Montpellier, France. [5]Faculté de Médecine Dentaire and Réseau de Recherche en Santé Bucco-dentaire et Osseuse du Fonds de Recherche Québec-Santé, Université de Montréal, Montréal, Québec, Canada. Correspondence should be addressed to A.K. (arlette.kolta@umontreal.ca).

Received 12 February; accepted 2 April; published online 4 May 2015; doi:10.1038/nn.4013

the trigeminal system and if they can be elicited by more physiological stimuli. We first tested the effects of electrical stimulation of the trigeminal tract on $[Ca^{2+}]_e$ and on neuronal firing. The trigeminal tract contains fibers of sensory afferents that project to NVsnpr. Ion-sensitive electrodes were used to monitor $[Ca^{2+}]_e$ following repetitive stimulation of the tract at 40 Hz, a frequency close to the sensory afferents' natural firing frequency during mastication[12]. To avoid possible washout of small external Ca^{2+} changes that could result from the rapid perfusion in a submerged preparation chamber, we conducted these experiments in a Haas-type interface chamber, where preparations were maintained at the interface between a warm, humidified atmosphere of O_2/CO_2 and a perfusing artificial cerebrospinal fluid (aCSF) containing 1.6 mM Ca^{2+} (**Fig. 1a**). However, only extracellular recordings can be conducted in this condition. In 14 of 22 cells, repetitive stimulation of the trigeminal tract produced long-lasting (≥30 min) decreases of $[Ca^{2+}]_e$ in dorsal NVsnpr (average drop: 1.1 ± 0.1 mM; **Fig. 1b**), while in the remaining 8 cases, no changes could be detected. In 9 of those 14 cases, $[Ca^{2+}]_e$ dropped below 0.4 mM (average drop of 1.3 ± 0.1 mM), and in all of these 9 cases, the firing pattern of neurons recorded extracellularly near the Ca^{2+}-sensitive electrode changed from tonic to rhythmic bursting (**Fig. 1c**,**d**). In the remaining 5 cases, the Ca^{2+} drop was of smaller amplitude (0.7 ± 0.1 mM) and no changes were observed on firing patterns of adjacent cells recorded. Firing patterns considered as rhythmic bursting and as tonic firing are illustrated in **Supplementary Figure 1** and the criteria used to distinguish them are described in Online Methods. Bursting occurred at an average frequency of 8.56 Hz ± 1.02 (**Supplementary Table 1**), well within the frequency range of bursts observed by electromyography in the jaw muscles of freely chewing rats (5–11 Hz, with a mean of 8.5 Hz)[13].

We then sought a robust stimulus to induce bursting and $[Ca^{2+}]_e$ decreases in submerged preparations, in order to conduct whole-cell recordings and Ca^{2+} imaging. In a previous study we had shown that rhythmic bursting elicited in NVsnpr neurons following stimulation of sensory afferents is blocked by an antagonist of NMDA receptors, DL-2-amino-5-phosphonopentanoic acid (APV), suggesting that these receptors are involved in burst induction[14]. Hence, we assessed in both interface and submerged slice preparations whether $[Ca^{2+}]_e$ and neuronal firing pattern would be altered by local applications of NMDA (1–2 mM). In interface preparations (n = 12 cells in 12 slices from 12 animals), local NMDA application elicited rhythmic bursting at frequencies (7.43 ± 1.2 Hz) close to those of rhythmic bursting elicited by stimulation of sensory afferents (**Supplementary Table 1**). In submerged preparations, similar NMDA applications produced $[Ca^{2+}]_e$ decreases (0.89 ± 0.11 mM; n = 8) (**Fig. 1e**) of shorter duration than those elicited by stimulation of sensory fibers in the interface chamber (23.69 ± 4.58 s). When applied near a neuron held at its resting membrane potential, NMDA caused a long-lasting depolarization

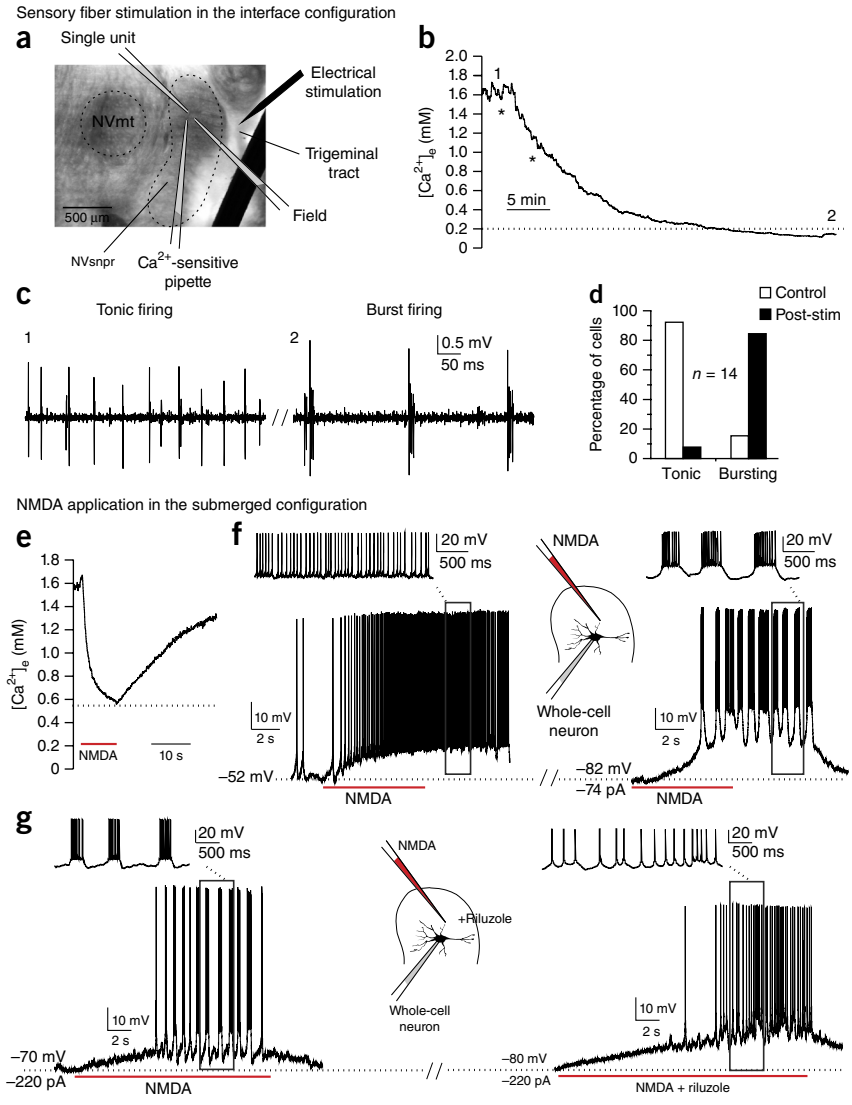

Figure 1 Sensory fibers stimulation and local NMDA application lead to $[Ca^{2+}]_e$ decreases and I_{NaP}-dependent neuronal bursting. (**a**) Stimulating and recording electrodes arrangement used in the interface chamber superimposed on a brainstem slice photomicrograph. NVmt, trigeminal motor nucleus. (**b**) Electrical stimulation (*, 1-s trains at 40 Hz) of sensory fibers in the trigeminal tract caused a long-lasting decrease in $[Ca^{2+}]_e$ (n = 14 of 22 recording locations in 18 slices from 14 rats). (**c**) Example of a neuron with a firing pattern that was tonic before stimulation (1) and became rhythmically bursting (2) when $[Ca^{2+}]_e$ dropped to under 0.3 mM (dotted line in **b**). (**d**) Firing pattern prevalence before (control) and after stimulation (post-stim) of the tract (see also **Supplementary Fig. 1**). (**e**) In submerged preparations, local application of NMDA (1 mM) also caused a decrease in $[Ca^{2+}]_e$ (n = 8 applications in 2 slices from 2 rats). (**f**) Left, at resting membrane potential, such applications produced a large depolarization and an increase in firing frequency, but no bursting (see inset) (1 mM: n = 5 cells in 3 slices from 3 rats; 2 mM: n = 3 cells in 3 slices from 1 rat). Right, rhythmic bursting (inset) was induced if the neuron was hyperpolarized by current injection before the application. (**g**) Rhythmic bursting induced by local application of NMDA (1 mM; left) was prevented when a blocker of I_{NaP} channels, riluzole (20 µM), was added to the bath (right). In this condition, NMDA no longer induced bursting, but was still strongly depolarizing and excitatory (n = 3 cells in 3 slices from 3 rats).

and induced firing, but the firing pattern remained tonic ($n = 5$ of 5 at 2 mM and 3 of 3 at 1 mM) (**Fig. 1f**). Rhythmic bursting (**Supplementary Table 1**) occurred only if the neurons were hyperpolarized before NMDA application ($n = 37$ at 2 mM, $n = 54$ at 1 mM in slices from 74 animals) (**Fig. 1f**) and showed the same voltage dependency as I_{NaP}-mediated events (namely, between −65 mV and −50 mV)[15] (**Supplementary Table 1**). Further, this NMDA-induced bursting was abolished by two I_{NaP} blockers, TTX (1 µM; $n = 5$ cells in 5 slices from 5 animals; data not shown) and riluzole (20 µM; $n = 3$; **Fig. 1g**).

I_{NaP}-mediated bursting is modulated by $[Ca^{2+}]_e$ but not $[Ca^{2+}]_i$

The above results suggest that bursting is associated with decreases in $[Ca^{2+}]_e$, but do not discriminate between the extracellular $[Ca^{2+}]$ or the potential subsequent fluctuation of intracellular $[Ca^{2+}]$ as the factor that promotes bursting. Under control conditions, when using a physiological $[Ca^{2+}]_e$ (1.6 mM)[16] in the perfusing medium, most neurons had a tonic firing pattern when activated with intracellular current injections or when firing spontaneously. Their firing pattern switched to rhythmic bursting when the perfusing medium was changed to a Ca^{2+}-free aCSF ($n = 12$; **Fig. 2a** and **Supplementary Table 1**) even though no changes were observed in their resting membrane potential (−53 ± 1 mV in 1.6 mM Ca^{2+} aCSF versus −54 ± 2 mV in Ca^{2+}-free aCSF; paired *t*-test; $P = 0.364$; $n = 12$) and in their input resistance (276 ± 55 MΩ in controls versus 267 ± 51 MΩ in Ca^{2+}-free aCSF; paired *t*-test; $P = 0.81$; $n = 10$). Even more confined Ca^{2+} reductions of shorter duration induced by local extracellular application of the Ca^{2+} chelator BAPTA (5–35 mM) near the recorded neurons induced rhythmic bursting ($n = 13$ of 13; **Fig. 2b**). In contrast, depletion of neuronal intracellular Ca^{2+} ($[Ca^{2+}]_i$) by addition of BAPTA (10–35 mM) to the solution used in the recording electrode did not induce bursting in neurons firing tonically under physiological $[Ca^{2+}]_e$ ($n = 11$) (**Fig. 2c**) and did not prevent NMDA-induced bursting ($n = 3$ of 3) (**Fig. 2c**). As with NMDA, bursts induced by local applications of extracellular BAPTA were I_{NaP}-dependent, as they were abolished by riluzole ($n = 5$ of 6; **Fig. 2d**).

Low $[Ca^{2+}]_e$ has been reported to enhance I_{NaP} (refs. 9,11,17,18). To ensure that this is the case here, we performed a series of voltage clamp experiments in a modified aCSF (see Online Methods) to pharmacologically block Ca^{2+} and K^+ conductances and isolate Na^+ currents. A slow voltage ramp (18 mV/s, 5 s) was used to activate I_{NaP} without activating fast sodium currents. In 11 dorsal NVsnpr neurons tested, the slow voltage-clamp command produced an inward sodium current (**Supplementary Fig. 2a**). Local application of extracellular BAPTA (10 mM) during the ramp protocol ($n = 6$) increased the peak of this inward current (**Supplementary Fig. 2b**) by 58 ± 13%. Peak currents were obtained at −44.7 ± 1.3 mV under control conditions and at −48.5 ± 1.7 mV with BAPTA, a shift of 8%. This inward current was blocked with bath application of riluzole (20 µM; $n = 4$ cells in 4 slices from 3 rats) or TTX (1–2 µM; $n = 2$ cells in 2 slices from 1 animal). We subtracted the trace obtained with a blocker (riluzole or TTX) from the trace obtained under control conditions or the trace obtained with BAPTA to isolate the I_{NaP} current observed in control conditions and in presence of BAPTA, respectively (**Supplementary Fig. 2c**). The characteristics of this isolated I_{NaP} current were obtained with the fitting of a single Boltzmann function to the normalized (to g_{max}) conductance-voltage data (**Supplementary Fig. 2d**). Taken together, these results strongly suggest that extracellular decrease of $[Ca^{2+}]$ promotes bursting and enhances I_{NaP} currents.

A recent report showed that decreasing $[Ca^{2+}]_e$ alters neuronal discharge through an astrocytic ATP-dependent mechanism[19]. To verify whether bursting induced by decreases in Ca^{2+} somehow involve ATP release and purinergic receptors, we assessed the effects of bath-applied suramine, a broad-spectrum antagonist of purinergic receptors (50 µM for >1 h). We found no effects on bursting induced by application of extracellular BAPTA (10 mM) in 5 of 5 cells (**Supplementary Fig. 3**).

Astrocytes respond to burst-inducing stimuli

Since regulation of extracellular ions is a key mechanism by which astrocytes affect neuronal functions[20], we hypothesized that astrocytes

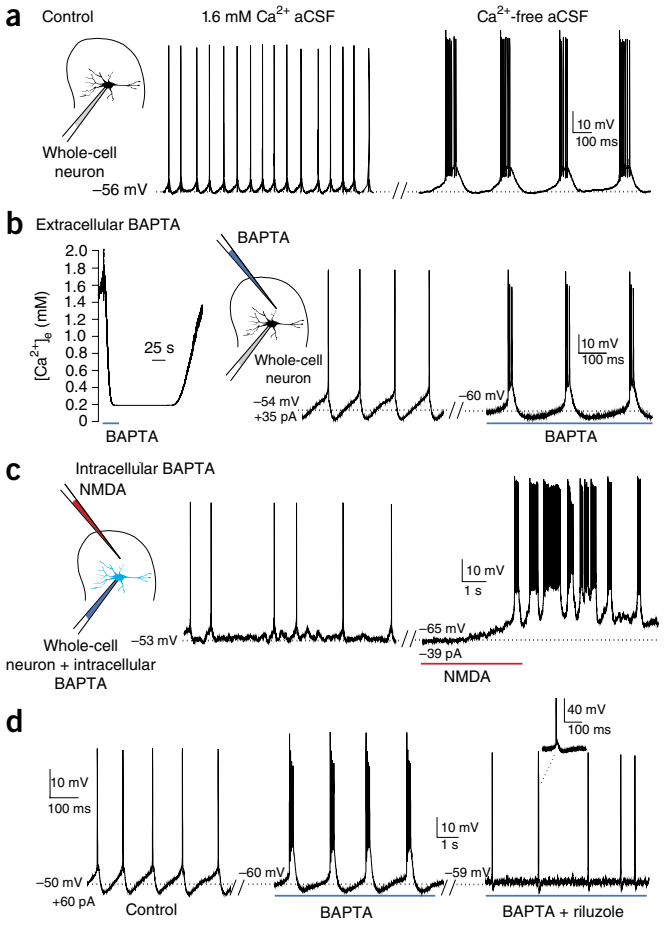

Figure 2 Reduction of extracellular Ca^{2+} leads to I_{NaP} dependent bursting independently of effects on intracellular Ca^{2+}. (**a**) The tonic firing pattern of NVsnpr neurons recorded under physiological $[Ca^{2+}]_e$ (1.6 mM; left) switches to burst firing when the perfusing medium is replaced by a Ca^{2+}-free medium ($n = 12$ cells in 10 slices from 10 rats). (**b**) Local extracellular application of BAPTA (10 mM; submerged preparation) produced a large but transient decrease of $[Ca^{2+}]_e$ (left) and induced rhythmic bursting (right) in an adjacent NVsnpr neuron that was firing tonically (middle) before the application ($n = 13$ cells in 9 slices from 9 rats). (**c**) The switch is not due to lack of intracellular Ca^{2+}, because chelation of neuronal intracellular Ca^{2+} by adding BAPTA (35 mM) to the recording pipette solution did not induce rhythmic bursting in a neuron firing tonically under physiological $[Ca^{2+}]_e$ (1.6 mM; left, $n = 11$ cells in 11 slices from 7 rats) and did not prevent NMDA-induced recurrent bursting in the same neuron (right, $n = 3$ cells in 3 slices from 3 rats). (**d**) Local extracellular application of BAPTA (10 mM) near a tonically firing NVsnpr neuron (left) induced rhythmic bursting (middle) under control conditions, but not in presence of riluzole (20 µM; right) in the bath. In the presence of riluzole, BAPTA had an effect on the spike after hyperpolarization, but little effect on the firing pattern ($n = 5$ of 6 cells in 6 slices from 5 rats).

may influence neuronal bursting by regulating $[Ca^{2+}]_e$. In this case, they should respond to the two stimuli (NMDA and sensory stimulation) that induce $[Ca^{2+}]_e$ decreases and neuronal bursting. We identified astrocytes by specific loading of sulforhodamine 101 (SR101; 1 µM in the bath) and their lack of active membrane properties (**Fig. 3a**). Using simultaneous whole-cell patch recordings and Ca^{2+} imaging, we observed that local NMDA (1 mM) applications produced large increases of intracellular Ca^{2+} (143.2 ± 28.8% $\Delta F/F_0$) accompanied by depolarizations (6.6 ± 1.2 mV; n = 5 astrocytes; **Fig. 3b**) under current clamp conditions. Consistently, repetitive stimulation (40–60 Hz; n = 5) of the glutamatergic[21] sensory fibers also depolarized NVsnpr astrocytes (**Fig. 3b**). Addition of TTX (1 µM) to the perfusing medium had little effect on the amplitude of the NMDA-induced membrane depolarization in astrocytes (**Fig. 3c**,**e**; n = 9 of 9), while addition of a mix of drugs blocking AMPA receptors, sodium channels, calcium channels and glutamate uptake (CNQX 10 µM, TTX 1 µM, cadmium 100 µM and L-*trans*-pyrollidine-2,4-dicarboxylic acid (PDC) 50 µM) reduced the NMDA-induced response by 53% on average (**Fig. 3d**,**e**; n = 5) and abolished (n = 2) or greatly reduced (by 93%; n = 1) synaptic responses to electrical stimulation of the sensory fibers (**Fig. 3d**,**e**). The remaining response to NMDA with the mix of blockers present presumably resulted from isolated NMDA-evoked current. To further test whether NVsnpr astrocytes express functional NMDA receptors, the NMDA receptor antagonist MK-801 (2 mM) was added to the internal recording solution. In 11 astrocytes recorded in this condition, NMDA applied locally elicited no response in 8 of the cells and a small depolarization in the 3 remaining cells. These depolarizations occurred only in the first minutes after initiating recording and disappeared after a few minutes of diffusion of MK-801 (**Fig. 3f**), while responses to local application of glutamate (1 mM), used as a control to test viability of the recorded cells, persisted in all 11 cells (**Fig. 3f**). These results clearly demonstrate that NMDA-induced activation of astrocytes does not depend on neuronal transmission and is at least partially mediated by direct activation of astrocytic NMDA receptors.

Inactivation of astrocytes prevents neuronal bursting

Astrocytes are coupled through gap junctions and form syncytia, as shown by dye diffusion (**Fig. 4a**). Hence a Ca^{2+}-chelating agent introduced in one astrocyte by a patch pipette will diffuse to neighboring astrocytes[22] and prevent astrocytic activity resulting from changes in cytosolic Ca^{2+}. Under control conditions, local application of NMDA induced widespread Ca^{2+} responses in cells loaded with a membrane-permeant Ca^{2+} indicator that were also positively labeled as astrocytes

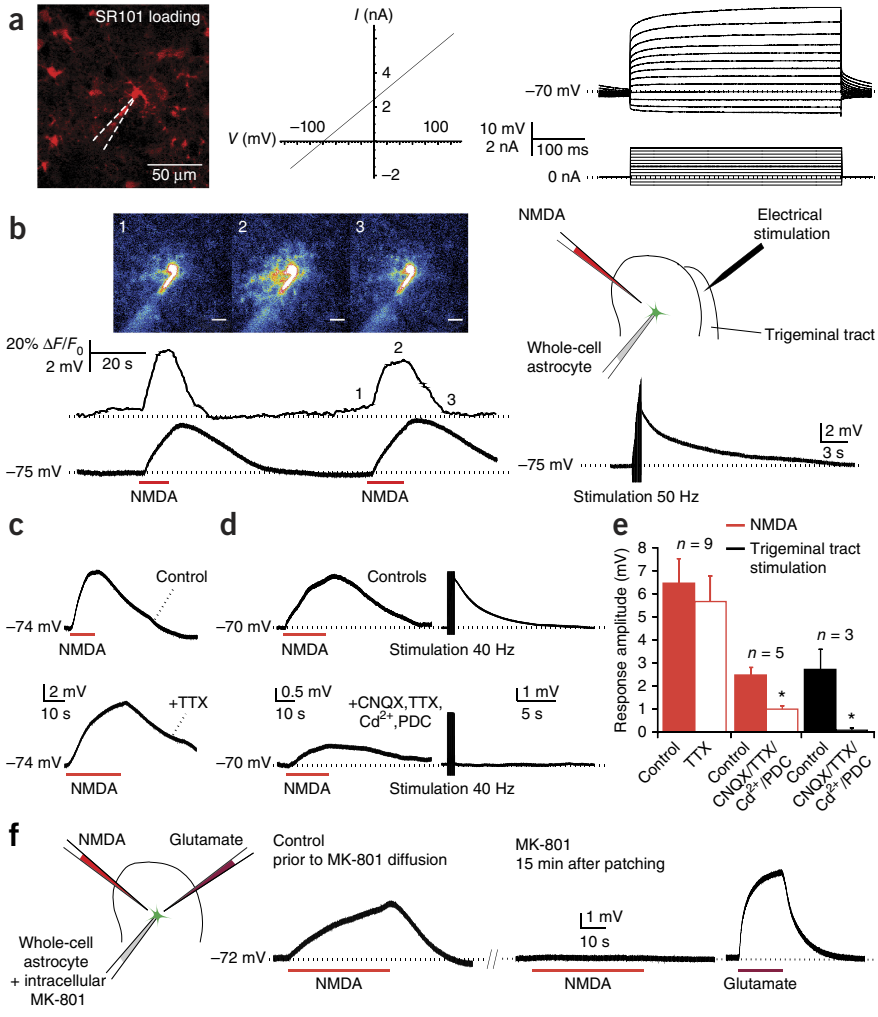

Figure 3 NVsnpr astrocytes have functional NMDA receptors and are activated by stimuli that cause $[Ca^{2+}]_e$ decreases and elicit neuronal rhythmic bursting. (**a**) Astrocytes were identified on the basis of their typical linear passive characteristics when imposing a depolarizing ramp from −130 mV to 110 mV in voltage clamp mode (middle) and the lack of action potentials in current clamp mode (right). In some experiments (left), the specific marker SR101 (red) was also used. (**b**) Repeated local NMDA applications induced reproducible Ca^{2+} responses (left: top and middle, fluo-4; 100 µM) and concomitant membrane depolarizations (bottom left) (n = 5 astrocytes in 5 slices from 4 rats), while 50 Hz stimulation of the trigeminal tract induced membrane depolarizations of astrocytes (bottom right, n = 5 cells in slices from 5 rats). Scale bars, 10 µm. (**c**) Depolarizations induced by local applications of NMDA under control conditions (top) and in presence of TTX (bottom) (1 µM) (n = 9 of 9 cells in 9 slices from 6 rats). (**d**) Depolarizations induced by local applications of NMDA (left, n = 5 cells in 5 slices from 5 rats) and stimulation of sensory afferents at 40 Hz (right, n = 3 cells in 3 slices from 2 rats) under control conditions (top) and in presence of a mix of drugs (bottom) blocking AMPA receptors (CNQX, 10 µM), glutamate uptake (PDC, 50 µM), Ca^{2+} channels (Cd^{2+}, 100 µM) and Na^+ channels (TTX, 1 µM). (**e**) Histograms show the effects of the different blockers on the amplitude of the depolarizations elicited by NMDA (paired t-test; P = 0.002) or sensory fibers stimulation (paired t-test; P = 0.043). *P < 0.05. (**f**) Local applications of NMDA (1 mM) caused membrane depolarization in an astrocyte immediately after entering the cell with a pipette filled with the NMDA receptor antagonist MK-801 (left), but no longer did so after 15 min of diffusion of MK-801 (middle), while glutamate (1 mM), which was used to ensure viability of the cell, still elicited a robust response after 15 min of diffusion (right) (n = 11 cells in 9 slices from 6 rats).

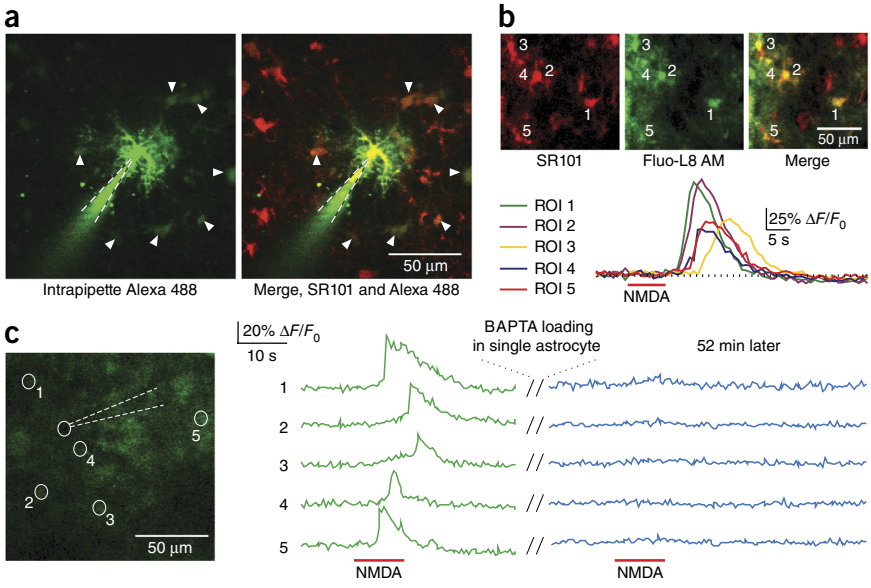

Figure 4 NVsnpr astrocytes are coupled and can be inactivated by introduction of BAPTA to the syncytium. (**a**) Coupling between astrocytes is revealed by diffusion of the tracer Alexa 488 (green; 100 µM) added to the internal solution of an electrode used to patch a single astrocyte and spreading to neighboring astrocytes (arrowheads) preloaded with SR101 (red) (double-labeled cells, right). (**b**) Single local NMDA application elicited Ca^{2+} responses in several astrocytes, as shown by the colocalization (merge) of the membrane-permeant indicator fluo-L8 AM (green) with SR101 (red) in the top panel. Bottom, Ca^{2+} responses in different astrocytes defined in regions of interest (ROI). (**c**) After incubation with fluo-L8 AM, several cells (circles and numbers, left) responded to a single NMDA application (green traces). Ca^{2+} responses to NMDA application were blocked in all cells after patching a single astrocyte with a BAPTA-filled (20 mM) pipette (blue traces). Mean intracellular Ca^{2+} increase before BAPTA, $\Delta F/F_0$ 51.3 ± 4%; after BAPTA, 14.2 ± 3%; $n = 26$ cells, paired t-test; $P = 1.082 \times 10^{-7}$.

with SR101 (**Fig. 4b**). However, BAPTA introduced in a single astrocyte prevented Ca^{2+}-dependent astrocytic activation of nearby astrocytes that were presumably coupled (**Fig. 4c**). Indeed, throughout 8 experiments with NMDA application per experiment, a total of 26 cells showed an intracellular Ca^{2+} increase in response to NMDA. Patching a single astrocyte in each experiment with a BAPTA-loaded electrode (20–35 mM) resulted in a loss of >75% of the original response to NMDA in 23 of the 26 cells.

To test whether inactivation of the astrocytic syncytium interferes with neuronal bursting, we performed dual recordings of a neuron and an adjacent astrocyte and assessed the neuronal bursting ability when BAPTA was added in the electrode used to record from the astrocyte. In 19 such pairs, local application of NMDA in the first few minutes of recording depolarized both the astrocyte and the neuron and led to rhythmic bursting if the neuron had been hyperpolarized before the application (**Fig. 5a**,**b**). By contrast, in 16 of the 19 pairs, NMDA still depolarized neurons and astrocytes after diffusion of BAPTA in the syncytium but could no longer elicit rhythmic bursting (**Fig. 5a–c**), even when further hyperpolarization was imposed on the neuron. In the 3 remaining cases, NMDA applications still elicited bursting even after BAPTA diffusion in the syncytium. This apparent lack of effect may result from impaired network integrity in the slice preparation. It is noteworthy that repeated NMDA applications caused reproducible bursting in neurons and Ca^{2+} increases in astrocytes recorded under control conditions over extended periods of time (**Fig. 5d**). In 3 more pairs in which either a second neuron, another type of glial cell or a distant astrocyte was inadvertently patched and dialyzed with BAPTA, NMDA-induced neuronal bursting persisted even after up to 90 min of BAPTA diffusion. In 4 more paired recordings, dialysis of the astrocytes with a much lower concentration of BAPTA (0.1 mM) did not alter neuronal bursting for over 60 min (**Supplementary Fig. 4a**).

Knowing that astrocytes are important for bursting and that reduction of $[Ca^{2+}]_e$ facilitates I_{NaP}-mediated bursting, we postulated that artificially reducing $[Ca^{2+}]_e$ should occlude the effect of BAPTA diffusion in the astrocytic syncytium. Indeed, in 3 pairs recorded in Ca^{2+}-free aCSF, neuronal bursting persisted after letting BAPTA (20 mM) diffuse in the astrocytic syncytium for more than 1 h (**Supplementary Fig. 4b**).

S100β induces bursting, reduces $[Ca^{2+}]_e$ and enhances I_{NaP}

We next investigated the mechanisms by which astrocytes could alter $[Ca^{2+}]_e$. The astrocytic protein S100β is a prime candidate owing to its glial specificity, its established Ca^{2+}-binding properties and its secretion by astrocytes[23,24]. As expected, immunostaining with an antibody directed against S100β revealed numerous immunoreactive astrocytes in dorsal NVsnpr (**Supplementary Fig. 5**; $n = 2$ animals). To assess the effects of this protein, we first synthesized it using a recombinant approach and tested its binding to Ca^{2+} with isothermal titration calorimetry (ITC). A clear endothermic binding of calcium to this S100β was observed with an apparent dissociation constant (K_d) of 25 µM and a stoichiometry of two calcium molecules for each molecule of protein, indicating that the synthesized S100β adopts its calcium-bound form (**Supplementary Fig. 6a**).

To test the effects of S100β on neuronal firing and on $[Ca^{2+}]_e$, we suspended the synthesized protein in a 20 mM HEPES buffer containing 140 mM NaCl and applied it locally at 129 µM in the submerged recording chamber and 50 µM in the interface chamber. In this initial set of experiments, the buffer used to suspend S100β was devoid of Ca^{2+} to prevent saturation of the protein and preserve its Ca^{2+}-binding ability. Consistent with this ability, we found that S100β applied locally in submerged preparations (bathed in aCSF containing 1.6 mM Ca^{2+}) caused large decreases in $[Ca^{2+}]_e$ as measured with ion-sensitive electrodes (reduction of 1.0 ± 0.1 mM, $n = 15$, **Fig. 6a**,**b**). As with BAPTA and NMDA, local extracellular applications of S100β caused neurons recorded in both interface and submerged chambers to change their firing pattern from tonic to rhythmic bursting ($n = 62$ of 76; **Fig. 6a**). Dual recordings of intracellular activity and $[Ca^{2+}]_e$ with ion-sensitive electrodes revealed that the transition from tonic to bursting firing appeared gradually and paralleled the Ca^{2+} decrease (**Fig. 6a**,**b**, $n = 5$). Doublet firing (shown in **Supplementary Fig. 1** and described in Online Methods) appeared, intermingled with single spikes, at a $[Ca^{2+}]_e$ of 0.9 ± 0.27 mM. At higher concentrations, only tonic firing (single spikes) was observed, and at a $[Ca^{2+}]_e$ of 0.69 ± 0.19 mM, only doublets were observed. Bursts (plateaus with three or more spikes) mingled with doublets appeared at a $[Ca^{2+}]_e$ of 0.54 ± 0.16 mM, and only bursts were seen at a $[Ca^{2+}]_e$ of 0.4 ± 0.13 mM and less. Notably, the frequency of the S100β-induced bursting was similar to that of bursting

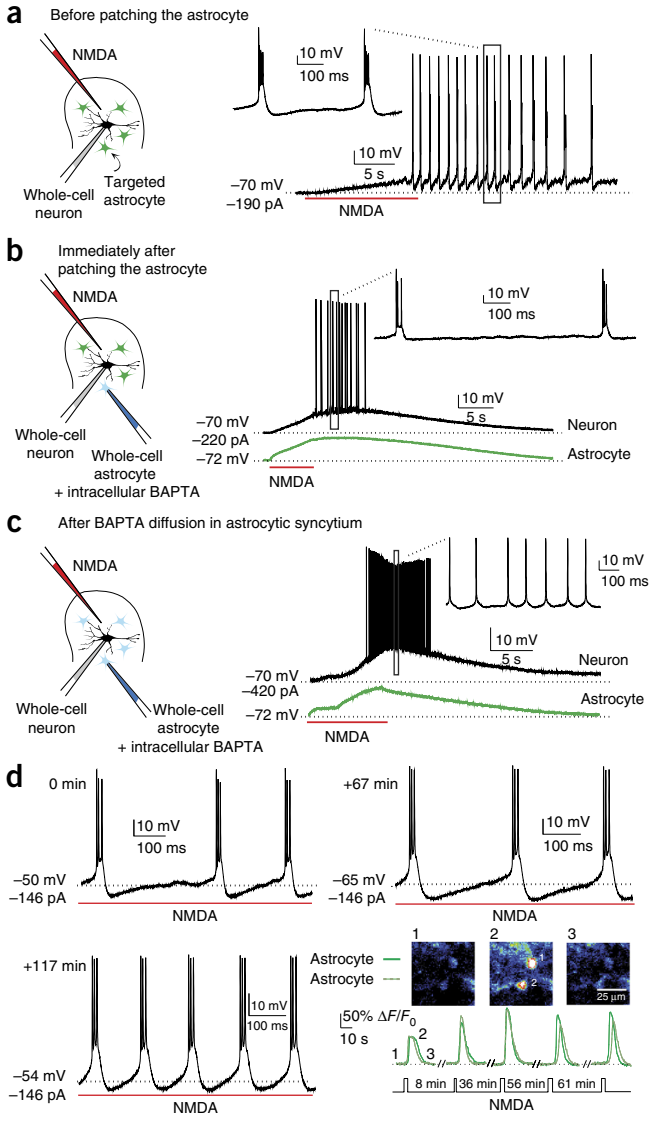

Figure 5 Inactivation of the astrocytic syncytium by diffusion of BAPTA impedes neuronal bursting. (**a**) Local NMDA application induced burst firing in an NVsnpr neuron before recording of an adjacent astrocyte with a BAPTA-filled pipette (20 mM). (**b**) NMDA applied immediately (<3 min) after entering the astrocyte with a BAPTA-filled electrode still elicited burst firing in the NVsnpr neuron (top), with a concomitant depolarization of the recorded astrocyte (green trace, bottom). (**c**) After diffusion of BAPTA in the astrocytic syncytium (>30 min), NMDA failed to elicit bursting, despite maintaining a depolarizing effect on the recorded neuron and astrocyte (n = 16 of 19 pairs in 19 slices from 19 rats). (**d**) In control conditions, rhythmic bursting could be elicited repetitively by NMDA applications in NVsnpr neurons recorded over long periods of time (here, 117 min). Similarly, calcium responses could be induced consistently in fluo-L8 AM–loaded astrocytes with repeated NMDA applications over long periods of time (bottom right). Calcium responses are shown in pseudocolor.

obtained following sensory fibers stimulation when tested in the interface chamber (7.47 ± 0.54 Hz versus 8.56 ± 1.03 Hz, respectively), as well as to that of NMDA-induced bursting when tested in submerged preparations (3.54 ± 0.53 versus 3.48 ± 0.71 for S100β versus NMDA, respectively; **Supplementary Table 1**).

S100β can have multiple effects, but the above results suggest that it promotes neuronal bursting by lowering $[Ca^{2+}]_e$. A series of experiments was undertaken to verify this and to determine whether the Ca^{2+}-free solution in which it was suspended had any effects on its own. First, local applications of the Ca^{2+}-free buffer alone caused a small decrease of $[Ca^{2+}]_e$ (0.55 ± 0.09 mM; n = 6; **Supplementary Fig. 7a**), but it did not alter the neuronal firing pattern in extracellular recordings in the interface chamber (n = 11; **Supplementary Fig. 7b**) and in intracellular recordings in the submerged configuration (n = 3; **Supplementary Fig. 7c**). Second, saturating the Ca^{2+}-binding activity of S100β by increasing to 2.6 mM the $[Ca^{2+}]$ in the circulating aCSF prevented induction of bursting by local applications of the protein suspended in Ca^{2+}-free solution (n = 4; **Supplementary Fig. 7d**). Similarly, S100β suspended in a buffer containing 1.6 mM Ca^{2+} had no effects on firing at the concentration used throughout the study (129 µM; n = 5; **Supplementary Fig. 7e**), and, as expected, the buffer alone containing 1.6 mM Ca^{2+} had no effect by itself on neuronal firing (n = 3 in 2 slices from 2 rats) and on $[Ca^{2+}]_e$ (n = 4 in 2 slices from 2 rats; data not shown). However, raising the concentration of the protein to 1 mM to overcome its saturation in the Ca^{2+}-containing buffer restored its effects on neuronal firing and on $[Ca^{2+}]_e$. Local applications of this solution containing 1 mM of S100β suspended in a buffer containing 1.6 mM $[Ca^{2+}]$ induced bursting in all 10 cells tested in the submerged configuration (**Supplementary Fig. 7e**) and caused large decreases in $[Ca^{2+}]_e$ (reduction of 1.27 ± 0.05 mM, n = 8 applications; **Fig. 6c**). Finally, to ensure that these effects of S100β could be attributed to its Ca^{2+}-binding ability, we tested the effects of an S100β protein with two mutated residues that obliterated its Ca^{2+} binding[25]. Local applications of a solution containing 1 mM of this mutated protein suspended in a 20 mM HEPES buffer containing 140 mM NaCl and 1.6 mM $CaCl_2$, had no effect on the neuronal firing pattern of the 7 cells recorded in the submerged configuration and caused only a marginal decrease of $[Ca^{2+}]_e$ (0.15 ± 0.02 mM; n = 7; **Fig. 6d**). These data provide very strong evidence that the effects of S100β on neuronal firing pattern result from its ability to bind Ca^{2+} and to decrease $[Ca^{2+}]_e$, which in turn enhances I_{NaP} and favors bursting. In all of the following experiments, S100β was used at the lower concentration (129 µM) in the submerged chamber and was suspended in the Ca^{2+}-free buffer.

We used riluzole to ascertain that the S100β-induced bursting involved I_{NaP}. Blockade of I_{NaP} channels with riluzole indeed prevented bursting induced by local application of S100β (**Fig. 6e**; n = 7 of 10 and 4 of 4 in interface and submerged preparations, respectively). In 3 cases, riluzole did not block the S100β-induced bursting, probably because of ineffective drug perfusion in the brain tissue, as these instances occurred only in the interface recording conditions.

To further assess whether the burst-inducing action of S100β could result from a modulation of I_{NaP}, we examined its effects on the pharmacologically isolated I_{NaP} current in voltage clamp experiments. As was the case for extracellular BAPTA, locally applied S100β (129 µM) significantly increased the peak amplitude of the isolated I_{NaP} by 55 ± 11% (n = 7; **Fig. 6e** and **Supplementary Fig. 2b**), and shifted the potential at which it occurred by 4%, or 2 mV (–44.7 ± 1.3 mV for controls versus –46.6 ± 1.9 mV for S100β). Again, the inward current induced by S100β was blocked with bath application of riluzole (20 µM; n = 3) or TTX (1–2 µM; n = 2 cells in 2 slices from 2 rats). The characteristics of this current assessed by fitting a Boltzmann function gave values between those obtained in controls and those obtained under BAPTA (**Supplementary Fig. 2d**).

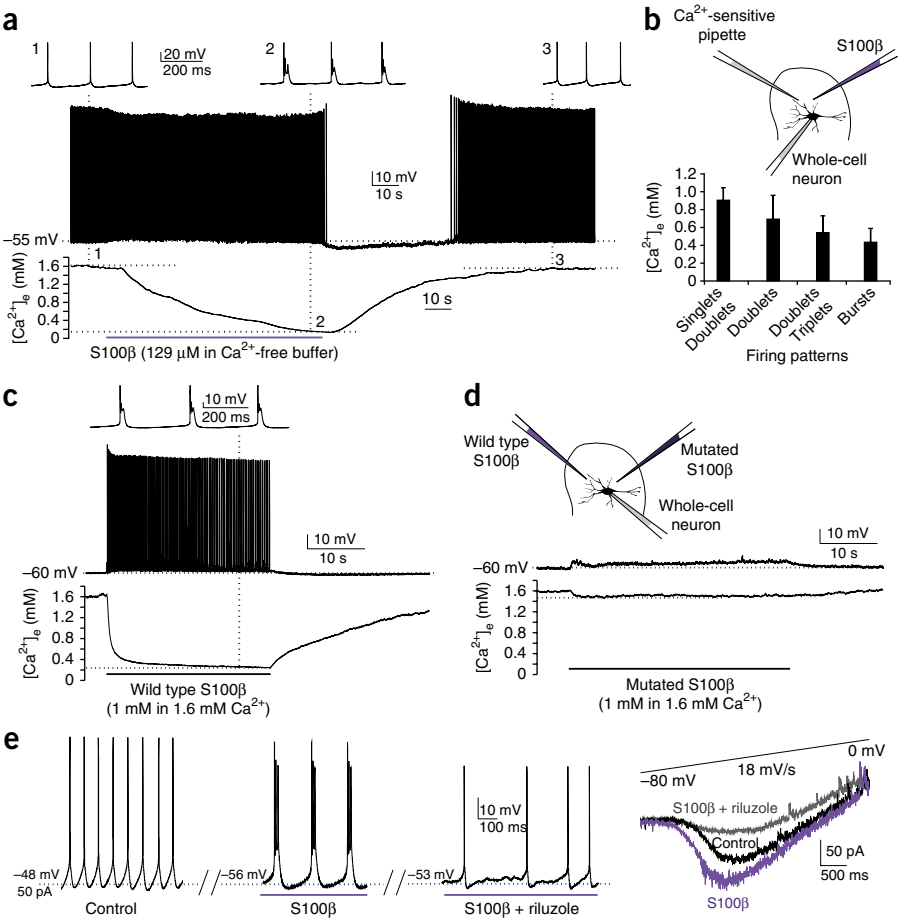

Figure 6 The astrocytic Ca^{2+} binding protein S100β causes $[Ca^{2+}]_e$ decreases and induces I_{NaP}-dependent bursting. (**a**) Local application of S100β (129 μM in Ca^{2+}-free buffer) near an NVsnpr neuron (left) in a submerged preparation causes a transient decreases of $[Ca^{2+}]_e$ (n = 15 $[Ca^{2+}]_e$ recording locations in 8 slices from 8 rats) and rhythmic bursting in an adjacent neuron (n = 62 of 76 cells in 66 slices from 57 rats). Insets (1, 2 and 3) show the firing pattern of the neuron on a larger time scale at the corresponding times on the $[Ca^{2+}]_e$ trace. (**b**) Histograms showing changes in firing pattern with $[Ca^{2+}]_e$ (n = 5 cells in 5 slices from 5 rats). (**c**) Similar effects on firing (n = 10 of 10 cells) and $[Ca^{2+}]_e$ (n = 8 recording locations) were elicited by local application of a wild-type S100β suspended in a solution containing 1.6 mM Ca^{2+}, but only if the concentration of the protein was raised to 1 mM to avoid its saturation (4 slices from 4 rats). (**d**) Local application of a recombinant S100β (1 mM in a buffer containing 1.6 mM Ca^{2+}) with two residues mutated to prevent Ca^{2+} binding had no effect on firing and caused only marginal changes in $[Ca^{2+}]_e$ (n = 7 cells and 7 adjacent $[Ca^{2+}]_e$ recording locations in 2 slices from 2 rats). (**e**) The S100β-induced bursting (middle) was abolished in the presence of the I_{NaP} blocker riluzole (20 μM, right, n = 11 of 14 cells in 14 slices from 11 rats). Left, voltage clamp recordings of a pharmacologically isolated inward current induced by a voltage ramp from –80 to 0 mV (top trace). The inward current elicited under control conditions (black) was increased by local application of S100β (purple; n = 7 cells in 7 slices from 5 rats; control, 88 ± 26 pA versus S100β, 135 ± 41 pA; paired t-test; P = 0.021) and blocked by riluzole (20 μM; gray, n = 3 cells in 3 slices from 2 rats).

If changes in neuronal firing and $[Ca^{2+}]_e$ induced by NMDA and sensory fibers stimulation depend on S100β, and if S100β release is downstream of NMDA and/or other glutamatergic receptors activation, then blocking Ca^{2+} responses in astrocytes with BAPTA should prevent NMDA-induced but not S100β-induced bursting. Indeed, in paired recordings of neurons and adjacent astrocytes with BAPTA in the electrode used for the astrocyte, either local applications of NMDA or of S100β induced rhythmic bursting in the first few minutes (**Fig. 7a**). NMDA-induced bursting was gradually blocked by diffusion of BAPTA in the astrocytic syncytium, whereas S100β-induced bursting persisted unaltered for as long as the cell was recorded (20–80 min after blockade of NMDA-induced bursting, n = 5 of 5; **Fig. 7b**).

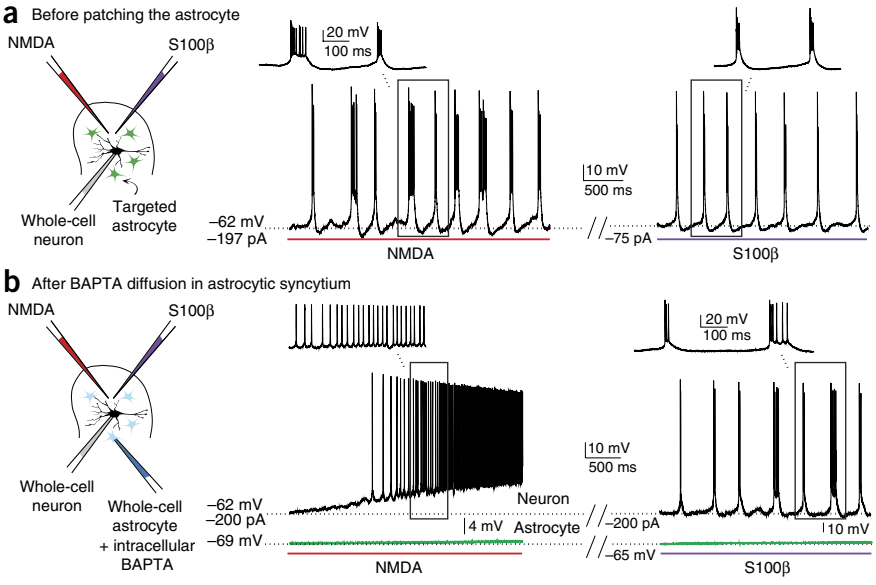

Figure 7 S100β-induced bursting persists after inactivation of the astrocytic syncytium with BAPTA. (**a**) Exogenously applied NMDA and S100β both induced burst firing in an NVsnpr neuron before dialysis of an adjacent astrocyte with BAPTA. (**b**) After BAPTA diffusion in the astrocytic syncytium, NMDA applied to the same neuron had a clear excitatory effect but no longer elicited rhythmic bursting (left), whereas S100β could still induce bursting (right) (n = 5 of 5 pairs in 5 slices from 5 rats).

Blockade of S100β prevents bursting induced by sensory fiber stimulation or NMDA

The above data suggest that S100β can still elicit bursting after inactivation of the astrocytic syncytium but do not prove that S100β

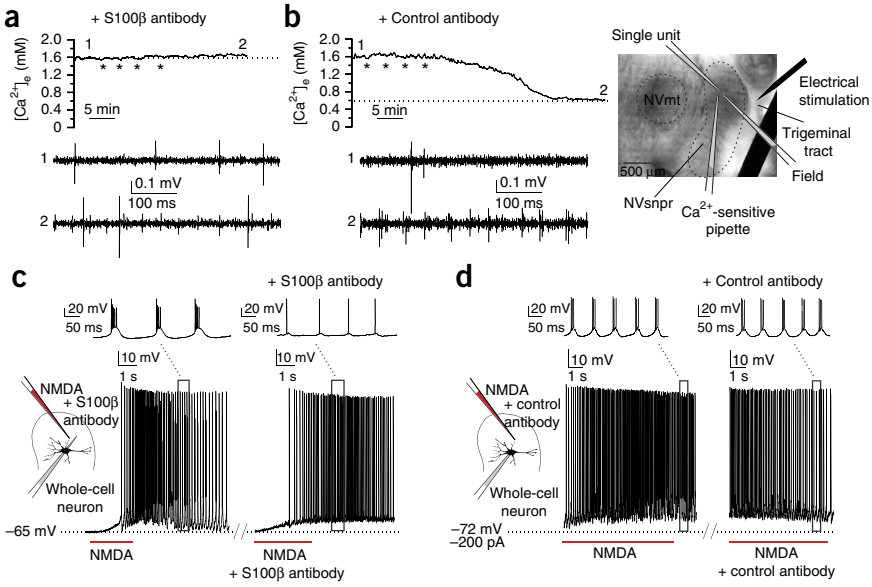

Figure 8 The presence of S100β in the extracellular space is required for bursting to occur in NVsnpr. (**a**) Inhibiting extracellular endogenous S100β activity with S100β antibody prevented the $[Ca^{2+}]_e$ decrease (top) following repetitive electrical stimulation (4 trains (*); 40 Hz, 1 s) of the trigeminal tract (n = 4 cells and 4 adjacent $[Ca^{2+}]_e$ recording locations in 4 slices from 3 rats). Bottom: in the same preparation, the tonic firing pattern of a spontaneously active neuron (1), recorded near the Ca^{2+}-sensitive electrode, was unaltered by the stimulation in presence of the antibody (2). 1 and 2 are recordings of the neuronal activity at times corresponding to 1 and 2 on the $[Ca^{2+}]$ record above. (**b**) Local application of an unrelated antibody (directed against sheep IgG) did not prevent the $[Ca^{2+}]_e$ decrease (top) and switch to burst firing (bottom) induced by repetitive stimulation of the trigeminal tract (*, 1-s trains at 40 Hz) (n = 2 cells and 2 adjacent $[Ca^{2+}]_e$ recording locations in 2 slices from 2 rats). (**c**) Similarly, in an NVsnpr neuron, NMDA-induced burst firing (left) was blocked by local application of anti-S100β antibody (40 μg/ml), resulting in tonic increase of firing without bursting (right) (n = 11 cells in 11 slices from 10 rats). (**d**) NMDA-induced rhythmic bursting (left) was unaltered by local application of the antibody against sheep IgG (n = 5 of 5 cells in 5 slices from 4 rats).

is required for bursting. We therefore tested whether blocking extracellular S100β activity with a local application of an S100β-subunit monoclonal antibody (40–80 μg/ml)[24] would prevent bursting induced by NMDA applications or sensory fiber stimulation. To insure that the antibody did interfere with the Ca^{2+}-binding ability of S100β, we used ITC. Indeed, no difference in the generated heat was observed when Ca^{2+} was added to S100β in the presence of the anti-S100β monoclonal antibody, indicating that binding of the antibody to S100β inhibited calcium binding (**Supplementary Fig. 6b**). In 4 of 4 slices examined in the interface chamber, pretreatment with this antibody before stimulation of the sensory fibers prevented neuronal bursting and $[Ca^{2+}]_e$ decreases measured with ion-sensitive electrodes (**Fig. 8a**). In 2 other cases, similar pretreatment with a nonspecific antibody (donkey anti–sheep IgG) did not prevent the Ca^{2+} decrease, nor the accompanying neuronal bursting (**Fig. 8b**) induced by sensory fibers stimulation. In 9 of 11 cells recorded in submerged slices, rhythmic bursting induced by NMDA was totally (n = 7; **Fig. 8c**) or partially (n = 2) blocked by treatment with the anti-S100β antibody. In the 2 cases considered partially blocked, NMDA applications elicited a few irregular bursts with a much shorter duration when compared to those elicited before application of the antibody. Use of the nonspecific antibody did not prevent bursting induced by NMDA in 5 of 5 cases (**Fig. 8d**). These data strongly suggest that sensory fibers stimulation and NMDA-induced neuronal bursting depend on the presence of S100β in the extracellular space and its capacity to bind Ca^{2+}.

DISCUSSION

The results presented here uncover a new mechanism for rhythmogenesis that depends on proper functioning of the astrocytes. The key element of this mechanism is regulation of I_{NaP}, the ionic conductance driving neuronal rhythmic burst firing, by decreases of $[Ca^{2+}]_e$. Changes in $[Ca^{2+}]_e$ follow stimulation of afferent inputs to NVsnpr neurons and result from activation of astrocytes and presumed subsequent release of the Ca^{2+}-binding protein S100β, which is required for bursting and $[Ca^{2+}]_e$ decreases to occur.

Physiological induction of $[Ca^{2+}]_e$ decreases and their implications for I_{NaP}-mediated bursting

Given the widespread importance of calcium signaling in numerous intracellular processes, studies have focused mainly on its regulation in the intracellular compartment. However, the imposition of artificial fluctuations in $[Ca^{2+}]_e$ in a variety of preparations have revealed marked effects of this ion on neuronal excitability. In an attempt to determine whether large changes in $[Ca^{2+}]_e$ can be expected to occur in the brain, Egelman and Montague[26], using a computational approach, concluded that large external Ca^{2+} fluctuations, leading to up to 100% depletion in many cases, must occur. Indeed, reductions in $[Ca^{2+}]_e$ have been reported to occur in parallel with $[K^+]_e$ increases during intense neuronal activity associated with seizures[10] or spreading depression[27], or with activity induced by massive electrical or pharmacological activation of the locomotor CPG[11] or electrical stimulation of the cerebellar cortex[28]. The $[Ca^{2+}]_e$ decreases reported in the above studies range between 0.1 mM and 0.7 mM and are of smaller magnitude than those reported here following stimulation of the trigeminal tract at a frequency close to the natural firing frequency of intra-oral afferents during mastication[12]. The difference in the measured $[Ca^{2+}]_e$ drops may result from various factors, including the age of the animal, the baseline $[Ca^{2+}]_e$ used and the positioning of the ion-sensitive electrode in relation to the location where the $[Ca^{2+}]_e$ drops occur.

How $[Ca^{2+}]_e$ drops affect bursting is not exactly known. Ca^{2+}-free perfusate has often been used to assess the role of synaptic transmission in various functions, and in many preparations this procedure leads to the appearance of spontaneous burst discharges[29,30]. Although a link between this bursting and I_{NaP} had been described in supraoptic neurons[17] and in hippocampus[18], it was established in CPGs only recently by us in the masticatory system[9] and later by others in the locomotor CPG[8,11]. This link is also likely to exist in at least part of the respiratory CPG, as low-Ca^{2+} perfusate is routinely used to obtain spontaneous bursting in *in vitro* preparations, including those of the pre-Bötzinger complex, where I_{NaP} is responsible for intrinsic bursting[30]. However, the fact that I_{NaP}-mediated bursting is facilitated

under low-Ca^{2+} conditions does not preclude the possibility that it may occur under physiological Ca^{2+} conditions as well. Indeed, our data from the sensory fiber stimulation suggest that neuronal activity can also produce Ca^{2+} decreases and I_{NaP} dependent bursting.

The interaction between Ca^{2+} and I_{NaP} is not fully understood, but work in the squid giant axon suggests that Ca^{2+} can occupy the pore of the sodium channel to favor its closing. In the absence of Ca^{2+}, closing slows or does not occur. The voltage sensitivity of closing kinetics also change with Ca^{2+} concentration and seem to depend in part on the ability of Ca^{2+} to enter and block the channels as voltage is driven negative[31]. This may partly explain why hyperpolarization was required to induce bursting when using NMDA. On one hand, hyperpolarization was required to keep the cells membrane potential within the I_{NaP} activation range by counteracting the depolarization induced by NMDA. On the other, it may have helped relieve the Ca^{2+} block of the Na^{+} channel. In neurons of the supraoptic nucleus, removal of external Ca^{2+} shifts the I_{NaP} activation threshold by ~13 mV towards more hyperpolarized potentials[17], while in Hb9 neurons of the locomotor CPG, every 0.1 mM decrease of Ca^{2+} shifts the I_{NaP} activation threshold and half-activation voltage by ~1 mV towards more hyperpolarized potentials; in both cases, I_{NaP} amplitude increases substantially[11]. This is in line with our data, wherein local applications of BAPTA and S100β, which both decrease $[Ca^{2+}]_e$, shifted the activation and half-activation voltage of I_{NaP} towards more hyperpolarized potentials. According to predictions based on a computational model of Hb9 cells, a slight shift of I_{NaP} activation would suffice to cause tonically firing neurons to burst rhythmically[11]. Here we found that bursting did not occur as long as $[Ca^{2+}]_e$ did not drop beneath 0.4 mM. Brocard *et al.*[11] were able to induce bursting in the locomotor CPG at a $[Ca^{2+}]_e$ of 0.9 mM, but only if $[K^{+}]$ was artificially raised to 6 mM. However, I_{NaP} currents were not upregulated by the increase of $[K^{+}]_e$. As suggested by Brocard *et al.*[11] and previous work from Rybak *et al.*[32], the facilitation seen with increased $[K^{+}]_e$ probably results from a change in the potassium equilibrium potential (E_K) that diminishes or suppresses a delayed-rectifier potassium current. Also, we cannot discard regional or age-related differences in I_{NaP} characteristics. Indeed, the mean peak amplitude that we observed was larger and occurred at more hyperpolarized potentials than those previously reported in NVsnpr neurons of younger animals (postnatal days 8–12)[33].

Function of astrocytes in regulating $[Ca^{2+}]_e$

Our data suggest that, in addition to activating NVsnpr neurons, stimulation of sensory afferents at a frequency close to their natural firing frequency[12] also activates astrocytes. Astrocytes have been shown to detect neurotransmitters release induced by basal[34] as well as intense neuronal activity[35] and to respond by releasing gliotransmitters, modulating neuronal activity in return. Here we show that NVsnpr astrocytes have functional NMDA receptors that enable them to respond to the glutamate released by afferent fibers. Astrocytes in other brain regions have also been reported to have functional NMDA receptors[36]. Locally applied NMDA may act on neuronal NMDA receptors and/or on these astrocytic NMDA receptors, causing release of other factors that may mediate burst induction. Rhythmic bursting induced by NMDA has traditionally been ascribed to the biphasic current-voltage (I-V) relationship of the current mediated by neuronal NMDA receptors[37,38]. However, although we cannot rule out involvement of all neuronal NMDA receptors, our observations suggest that NMDA receptors of the recorded neuron itself are unlikely to play a significant role, as neuronal NMDA receptors are normally blocked in hyperpolarized states and are mostly permeable to Ca^{2+}. The findings that hyperpolarization was required for burst induction and that the NMDA-induced bursting was insensitive to intraneuronal diffusion of BAPTA suggest that NMDA receptors located elsewhere than on the recorded neuron are likely to be involved in the observed bursting.

We postulate that activation of astrocytes through their NMDA receptors and/or other glutamatergic receptors leads to $[Ca^{2+}]_e$ decreases because (i) the astrocytic syncytium must be functional and (ii) $[Ca^{2+}]_e$ must decrease for bursting to occur. Modulation of $[Ca^{2+}]_e$ by astrocytes has often been postulated, but never demonstrated. The fact that exogenous applications of a Ca^{2+}-binding protein released by astrocytes, S100β[23,24], decreased Ca^{2+} and induced bursting even after inactivation of the astrocytic syncytium with BAPTA is a clear indication, but not proof, that astrocytes act by releasing S100β. However, the fact that blockade of this protein with a specific antibody prevents $[Ca^{2+}]_e$ decreases and bursting induced with sensory fibers stimulation and NMDA applications is strong evidence that S100β is required for bursting to occur. Furthermore, the secretion of S100β from astrocytes has been reported to be stimulated by glutamate receptors activation as well as by intracellular calcium increase[39], two conditions that are met in our experiments.

Surprisingly, despite its well-established Ca^{2+}-binding property, previous studies that have focused on S100β extracellular actions have not addressed a possible regulatory function of local extracellular Ca^{2+} concentration. Intracellularly, S100β carries out many regulatory activities through Ca^{2+}-dependent interactions with the cytoskeleton and with several cytoplasmic proteins involved in cell differentiation, proliferation and survival (for review, see ref. 39). Once released in the extracellular compartment, S100β carries out many actions via activation of RAGE (receptor for advanced glycation end products)[39]. We cannot rule out the possibility that these other effects of S100β are important, but we can affirm that its effects on extracellular Ca^{2+} are required for bursting. Indeed, S100β loses its ability to alter neuronal firing once mutated at its Ca^{2+}-binding sites, and inactivation of astrocytes with BAPTA in the Ca^{2+}-free condition did not alter bursting. This latter finding also suggests that no other gliotransmitters that may be released from astrocytes in a Ca^{2+}-dependent manner are required for bursting. In particular, our data argue strongly that ATP, a well-known gliotransmitter, is not likely to be involved owing to the lack of effect on neuronal bursting of suramine, a broad antagonist of purinergic receptors.

Functional significance: switch of neuronal function in territories defined by glial syncytia

On the basis of these results, we propose a model whereby sustained synaptic inputs to NVsnpr arriving at a physiologically relevant frequency (40–60 Hz) initiate rhythmogenesis by activating both neurons and astrocytes (**Supplementary Fig. 8**). Sporadic or low-frequency firing of the inputs is insufficient to activate the astrocytes. Under this condition, the circuit operates in a conventional sensory relay mode wherein the output is linearly related to the input (**Supplementary Fig. 8**). With more sustained activity at higher frequency, astrocytes are activated, couple to form a syncytium and release S100β. The extent of the syncytium would define a territory (**Supplementary Fig. 8**) within which the confined neurons will be exposed to the same decrease in $[Ca^{2+}]_e$ and, therefore, have the same conditions of activation or inactivation of I_{NaP} channels. The terminals of inputs to NVsnpr are highly organized[40] and are likely to activate adjacent neurons and astrocytes. Firing of these inputs could therefore act as a common trigger to initiate rhythmic activity in a given population of neurons, which will be synchronized

because they are surrounded by the same astrocytic syncytium. The population of rhythmogenic neurons could vary constantly and in an adaptive manner according to the pattern of incoming inputs. Notably, NVsnpr neurons also receive glutamatergic projections from the cortical masticatory area, known to be important for initiation of the movements and the first few cycles of a masticatory sequence[41]. Stimulation of this area elicits mastication *in vivo*, but only when trains of stimuli are delivered at frequencies between 20 and 100 Hz and optimally around 40–50 Hz (ref. 42). Thus, NVsnpr neurons could be considered an interface converting sensory and/or cortical inputs into rhythmic motor commands when astrocytes are activated by increased or coincident activity of these inputs. A similar role was assigned to the lamprey reticulospinal cells receiving sensory inputs from the trigeminal system[43]. This dual function of NVsnpr neurons is in line with their projections to the thalamus (sensory relay mode) and to brainstem motor neurons and premotor interneurons, on one hand, and with their two firing modes on the other. Interestingly, the bursting frequency of NVsnpr neurons reported during fictive mastication in rabbit (~3 Hz)[44] corresponds to the chewing frequency in that species. Similarly, the frequency of bursting elicited here in the interface chamber, whether by sensory stimulation, NMDA or S100β, corresponds to the chewing frequency observed *in vivo* in rats[13]. In submerged preparations, the bursting frequency was slower, but this probably results from differences in temperature between the two recording conditions (room temperature for submerged versus 30–32 °C for interface).

Implications for health and pathology

Astrocytes have many important functions, including at least one in a rhythmic circuit, the respiratory CPG, where they alter the inspiratory rhythm by releasing ATP[6] in response to a change in pH. However, in this case, the mechanism involved is pH dependent and seems specific to the ventral brainstem respiratory area[45], whereas the mechanism of action reported here may be of a much broader relevance given the widespread distribution of both S100β and I_{NaP} (refs. 4,8,9,11,17,18,30).

Regulation of I_{NaP}-mediated bursting by astrocytes may help explain the appearance of bursting in normal and pathological conditions, such as epileptic seizures, where astrocytes are overactivated[46]. Generation and propagation of seizures are generally attributed to spread of activity in excitatory feedback circuits. However, surprisingly, *in situ* measurements with ion-selective electrodes show that during seizures, $[Ca^{2+}]_e$ drops to levels incompatible with chemical synaptic transmission[47]. Our results may help explain this paradoxical finding and could explain how bursting activity is maintained in the absence of chemical synaptic transmission. These findings could help develop new targets and strategies for the treatment of these conditions.

METHODS

Methods and any associated references are available in the online version of the paper.

Note: Any Supplementary Information and Source Data files are available in the online version of the paper.

ACKNOWLEDGMENTS

This paper is dedicated to Laurent Vinay, whose premature loss leaves us with a tremendous void. To a great man who left his mark in this field by his science and his humanity. We are extremely grateful to D. Weber and P. Wilder from the Center for Biomolecular Therapeutics for generously providing the mutated S100β, which was well characterized in their previous work. We are equally grateful to J.G. Omichinski for giving us access to his Microcal ITC-200 microcalorimeter and for counseling us on these experiments. We also thank A. Panatier for counseling and assistance in several experiments on astrocytes and F. Amzica, who guided us for the ion-sensitive recordings. S. Condamine generously performed the immunostaining of S100β in NVsnpr. P.M. received a fellowship from the Network for Oral Health and Bone Health Research of the Fonds de Recherche Québec-Santé. This research was financed by a grant from the Canadian Institutes for Health Research (grant 14392).

AUTHOR CONTRIBUTIONS

The work presented here was carried out in collaboration between all authors. All authors have contributed to, seen and approved the manuscript. A. Kolta and R.R. cosupervised the project and worked together to define the research themes, design the experiments and draft the manuscript (writing and critical revision). P.M. co-designed and carried out the patch recording and Ca^{2+} imaging experiments and worked on the data analysis, the interpretation of the results, and the drafting of the manuscript (writing and figures conception). D.V. co-designed and carried out part of the patch recording experiments, co-designed and carried out the interface configuration experiments, and worked on the data analysis, interpretation of the results and drafting of the manuscript (writing and figure concepts). A. Kadala co-designed and carried out the calcium ion–sensitive recording experiments and worked on the data analysis, the interpretation of the results and the drafting of the manuscript (writing and figure concepts). J.F. synthesized the S100β and conducted the microcalorimetry experiments and analyzed the related data. A.G.P. carried out some of the patch experiments and worked on the data analysis.

COMPETING FINANCIAL INTERESTS

The authors declare no competing financial interests.

1. Grillner, S. Locomotion in vertebrates: central mechanisms and reflex interaction. *Physiol. Rev.* **55**, 247–304 (1975).
2. Dellow, P.G. & Lund, J.P. Evidence for central timing of rhythmical mastication. *J. Physiol. (Lond.)* **215**, 1–13 (1971).
3. Smith, J.C., Ellenberger, H.H., Ballanyi, K., Richter, D.W. & Feldman, J.L. Pre-Botzinger complex: a brainstem region that may generate respiratory rhythm in mammals. *Science* **254**, 726–729 (1991).
4. Harris-Warrick, R.M. General principles of rhythmogenesis in central pattern generator networks. *Prog. Brain Res.* **187**, 213–222 (2010).
5. Del Negro, C.A. *et al.* Synaptically activated burst-generating conductances may underlie a group-pacemaker mechanism for respiratory rhythm generation in mammals. *Prog. Brain Res.* **187**, 111–136 (2010).
6. Gourine, A.V. *et al.* Astrocytes control breathing through pH-dependent release of ATP. *Science* **329**, 571–575 (2010).
7. Okada, Y. *et al.* Preinspiratory calcium rise in putative pre-Botzinger complex astrocytes. *J. Physiol. (Lond.)* **590**, 4933–4944 (2012).
8. Tazerart, S., Vinay, L. & Brocard, F. The persistent sodium current generates pacemaker activities in the central pattern generator for locomotion and regulates the locomotor rhythm. *J. Neurosci.* **28**, 8577–8589 (2008).
9. Brocard, F., Verdier, D., Arsenault, I., Lund, J.P. & Kolta, A. Emergence of intrinsic bursting in trigeminal sensory neurons parallels the acquisition of mastication in weanling rats. *J. Neurophysiol.* **96**, 2410–2424 (2006).
10. Massimini, M. & Amzica, F. Extracellular calcium fluctuations and intracellular potentials in the cortex during the slow sleep oscillation. *J. Neurophysiol.* **85**, 1346–1350 (2001).
11. Brocard, F. *et al.* Activity-dependent changes in extracellular Ca^{2+} and K^+ reveal pacemakers in the spinal locomotor-related network. *Neuron* **77**, 1047–1054 (2013).
12. Trulsson, M. & Johansson, R.S. Orofacial mechanoreceptors in humans: encoding characteristics and responses during natural orofacial behaviors. *Behav. Brain Res.* **135**, 27–33 (2002).
13. Westneat, M.W. & Hall, W.G. Ontogeny of feeding motor patterns in infant rats–an electromyographic analysis of suckling and chewing. *Behav. Neurosci.* **106**, 539–554 (1992).
14. Bernier, A.P., Arsenault, I., Lund, J.P. & Kolta, A. Effect of the stimulation of sensory inputs on the firing of neurons of the trigeminal main sensory nucleus in the rat. *J. Neurophysiol.* **103**, 915–923 (2010).
15. Crill, W.E. Persistent sodium current in mammalian central neurons. *Annu. Rev. Physiol.* **58**, 349–362 (1996).
16. Jones, H.C. & Keep, R.F. Brain fluid calcium concentration and response to acute hypercalcaemia during development in the rat. *J. Physiol. (Lond.)* **402**, 579–593 (1988).
17. Li, Z. & Hatton, G.I. Oscillatory bursting of phasically firing rat supraoptic neurones in low-Ca^{2+} medium: Na^+ influx, cytosolic Ca^{2+} and gap junctions. *J. Physiol. (Lond.)* **496**, 379–394 (1996).
18. Su, H., Alroy, G., Kirson, E.D. & Yaari, Y. Extracellular calcium modulates persistent sodium current-dependent burst-firing in hippocampal pyramidal neurons. *J. Neurosci.* **21**, 4173–4182 (2001).

19. Torres, A. *et al.* Extracellular Ca^{2+} acts as a mediator of communication from neurons to glia. *Sci. Signal.* **5**, ra8 (2012).
20. Wang, F. *et al.* Astrocytes modulate neural network activity by Ca^{2+}-dependent uptake of extracellular K^{+}. *Sci. Signal.* **5**, ra26 (2012).
21. Lazarov, N.E. Comparative analysis of the chemical neuroanatomy of the mammalian trigeminal ganglion and mesencephalic trigeminal nucleus. *Prog. Neurobiol.* **66**, 19–59 (2002).
22. Serrano, A., Haddjeri, N., Lacaille, J.C. & Robitaille, R. GABAergic network activation of glial cells underlies hippocampal heterosynaptic depression. *J. Neurosci.* **26**, 5370–5382 (2006).
23. Ciccarelli, R. *et al.* Activation of A_1 adenosine or mGlu3 metabotropic glutamate receptors enhances the release of nerve growth factor and S-100beta protein from cultured astrocytes. *Glia* **27**, 275–281 (1999).
24. Sakatani, S. *et al.* Neural-activity-dependent release of S100B from astrocytes enhances kainate-induced gamma oscillations in vivo. *J. Neurosci.* **28**, 10928–10936 (2008).
25. Markowitz, J. *et al.* Calcium-binding properties of wild-type and EF-hand mutants of S100B in the presence and absence of a peptide derived from the C-terminal negative regulatory domain of p53. *Biochemistry* **44**, 7305–7314 (2005).
26. Egelman, D.M. & Montague, P.R. Calcium dynamics in the extracellular space of mammalian neural tissue. *Biophys. J.* **76**, 1856–1867 (1999).
27. Lian, X.Y. & Stringer, J.L. Astrocytes contribute to regulation of extracellular calcium and potassium in the rat cerebral cortex during spreading depression. *Brain Res.* **1012**, 177–184 (2004).
28. Nicholson, C., Bruggencate, G.T., Steinberg, R. & Stockle, H. Calcium modulation in brain extracellular microenvironment demonstrated with ion-selective micropipette. *Proc. Natl. Acad. Sci. USA* **74**, 1287–1290 (1977).
29. Jefferys, J.G. & Haas, H.L. Synchronized bursting of CA1 hippocampal pyramidal cells in the absence of synaptic transmission. *Nature* **300**, 448–450 (1982).
30. Del Negro, C.A., Morgado-Valle, C. & Feldman, J.L. Respiratory rhythm: an emergent network property? *Neuron* **34**, 821–830 (2002).
31. Armstrong, C.M. Distinguishing surface effects of calcium ion from pore-occupancy effects in Na^{+} channels. *Proc. Natl. Acad. Sci. USA* **96**, 4158–4163 (1999).
32. Rybak, I.A., Shevtsova, N.A., St-John, W.M., Paton, J.F. & Pierrefiche, O. Endogenous rhythm generation in the pre-Botzinger complex and ionic currents: modelling and in vitro studies. *Eur. J. Neurosci.* **18**, 239–257 (2003).
33. Tsuruyama, K., Hsiao, C.F. & Chandler, S.H. Participation of a persistent sodium current and calcium-activated nonspecific cationic current to burst generation in trigeminal principal sensory neurons. *J. Neurophysiol.* **110**, 1903–1914 (2013).
34. Panatier, A. *et al.* Astrocytes are endogenous regulators of basal transmission at central synapses. *Cell* **146**, 785–798 (2011).
35. Pasti, L., Volterra, A., Pozzan, T. & Carmignoto, G. Intracellular calcium oscillations in astrocytes: a highly plastic, bidirectional form of communication between neurons and astrocytes *in situ*. *J. Neurosci.* **17**, 7817–7830 (1997).
36. Lee, M.C. *et al.* Characterisation of the expression of NMDA receptors in human astrocytes. *PLoS ONE* **5**, e14123 (2010).
37. Sigvardt, K.A., Grillner, S., Wallen, P. & Van Dongen, P.A. Activation of NMDA receptors elicits fictive locomotion and bistable membrane properties in the lamprey spinal cord. *Brain Res.* **336**, 390–395 (1985).
38. Kim, Y.I. & Chandler, S.H. NMDA-induced burst discharge in guinea pig trigeminal motoneurons in vitro. *J. Neurophysiol.* **74**, 334–346 (1995).
39. Donato, R. *et al.* S100B's double life: intracellular regulator and extracellular signal. *Biochim. Biophys. Acta* **1793**, 1008–1022 (2009).
40. Capra, N.F. & Dessem, D. Central connections of trigeminal primary afferent neurons: topographical and functional considerations. *Crit. Rev. Oral. Biol. Med.* **4**, 1–52 (1992).
41. Yamamura, K. *et al.* Effects of reversible bilateral inactivation of face primary motor cortex on mastication and swallowing. *Brain Res.* **944**, 40–55 (2002).
42. Lund, J.P. & Dellow, P.G. The influence of interactive stimuli on rhythmical masticatory movements in rabbits. *Arch. Oral Biol.* **16**, 215–223 (1971).
43. Di Prisco, G.V., Pearlstein, E., Robitaille, R. & Dubuc, R. Role of sensory-evoked NMDA plateau potentials in the initiation of locomotion. *Science* **278**, 1122–1125 (1997).
44. Tsuboi, A., Kolta, A., Chen, C.C. & Lund, J.P. Neurons of the trigeminal main sensory nucleus participate in the generation of rhythmic motor patterns. *Eur. J. Neurosci.* **17**, 229–238 (2003).
45. Kasymov, V. *et al.* Differential sensitivity of brainstem versus cortical astrocytes to changes in pH reveals functional regional specialization of astroglia. *J. Neurosci.* **33**, 435–441 (2013).
46. Gomez-Gonzalo, M. *et al.* An excitatory loop with astrocytes contributes to drive neurons to seizure threshold. *PLoS Biol.* **8**, e1000352 (2010).
47. Pumain, R., Menini, C., Heinemann, U., Louvel, J. & Silva-Barrat, C. Chemical synaptic transmission is not necessary for epileptic seizures to persist in the baboon *Papio papio*. *Exp. Neurol.* **89**, 250–258 (1985).

ONLINE METHODS

Brainstem slice preparations. All procedures abided by the Canadian Institutes of Health Research rules and were approved by the University of Montreal Animal Care and Use Committee. Experiments were conducted on 15- to 21-day-old Sprague-Dawley rats anesthetized with isoflurane (Pharmaceutical Partners of Canada Inc., Richmond Hill, Ontario, Canada) before decapitation. Their brain was quickly removed from the cranium and dipped in an ice-cold sucrose-based solution consisting of (in mM) 3 KCl, 1.25 KH_2PO_4, 4 $MgSO_4$, 26 $NaHCO_3$, 10 dextrose, 0.2 $CaCl_2$, 219 sucrose bubbled with a mix of 95% O_2 and 5% CO_2, pH 7.3–7.4, 300–320 mosmol/kg. Transverse slices (300–400 µm thick) of the trigeminal main sensory nucleus (NVsnpr) were prepared in the same medium with a vibratome (Leica, model VT 100S). Slices were then stored and allowed to rest for an hour in a holding chamber filled with artificial cerebrospinal fluid (aCSF) at room temperature (95% O_2 + 5% CO_2). The aCSF consisted of (in mM) 124 NaCl, 3 KCl, 1.25 KH_2PO_4, 1.3 $MgSO_4$, 26 $NaHCO_3$, 10 dextrose and 1.6 $CaCl_2$, pH 7.3–7.4, 290–300 mosmol/kg. This composition of aCSF was used in all experiments throughout the study, except in experiments conducted to isolate I_{NaP} in voltage clamp (see below) and experiments where the $CaCl_2$ was either increased to 2.6 mM or omitted and replaced by $MgCl_2$ (1.6 mM). The experiments where such manipulations of the $[Ca^{2+}]$ were used are noted in the Results.

Electrophysiological recordings. *Interface configuration.* For experiments done in the interface chamber configuration, 400-µm-thick slices were kept at 30–32 °C at the interface between a warm humidified atmosphere of 95% O_2/5% CO_2 and aCSF. NVsnpr was identified under 4× magnification and extracellular field potential recording electrodes as well as calcium-sensitive electrodes (see details below) were placed in the dorsal part of the nucleus and connected through their own amplifiers to a Micro 1401 mk II acquisition unit (Cambridge Electronic Design, Cambridge, UK). All electrodes, except for the calcium-sensitive one, were filled with NaCl (0.5 M). An Isostim stimulator (model A320; WPI, Sarasota, FL, USA) and tungsten (unipolar) or nichrome (bipolar) electrodes were used to electrically stimulate (40–60 Hz) the sensory fibers in the trigeminal tract projecting to NVsnpr.

Submerged configuration. Whole cell experiments and calcium imaging recordings were conducted at room temperature in an immersion chamber using slices 300–350 µm thick. Neurons and astrocytes were visualized with an infrared-sensitive CCD camera and displayed on a video monitor. The camera was mounted on an Olympus FluoView FV 1000 confocal microscope equipped with a 40× water-immersion objective. Whole-cell recordings were performed in the current clamp mode or in the voltage clamp mode (see below) using a computer-controlled Multiclamp 700A amplifier and a Digidata 1322A digitizer (Axon Instruments, Downingtown, PA, USA). The apparatus was equipped with two headstages, allowing recordings of pairs of cells. Patch pipettes were pulled from borosilicate glass capillaries (1.5 mm OD, 1.12 mm ID; World Precision Instruments, Sarasota, FL) on a Sutter P-97 puller (Sutter Instruments, Novato, CA). Electrodes for neuronal recordings (resistance 7–10 MΩ) were filled with (in mM) 140 potassium gluconate, 5 NaCl, 2 $MgCl_2$, 10 HEPES, 0.5 EGTA, 2 Tris ATP salt, 0.4 Tris GTP salt, pH 7.2–7.3, 280–300 mosmol/kg. After the establishment of a gigaseal, the pipette resistance and capacitance were compensated electronically. Neurons were monitored throughout experiments to assess their viability and were discarded when action potentials did not overshoot 0 mV or when the resting membrane potential was depolarized (≥ –45 mV). Electrodes for astrocyte recordings (resistance 5–7 MΩ) were filled with (in mM) 125 KCH_3SO_4, 10 HEPES, 4 $MgCl_2$, 4 ATP, 0.4 GTP, 10 disodium creatine phosphate and 0.1 Alexa Fluor 488, pH 7.2–7.3, 295–300 mosmol/kg. For imaging experiments in single astrocytes, the Ca^{2+} indicator fluo-4 (100 µM) (Invitrogen) was added to the internal solution and Alexa Fluor 488 was omitted. Astrocytes were identified on the basis of their small size (~10 µm) and characteristic morphology of a round soma surrounded by many processes. In some experiments, sulforhodamine 101 (SR101, 1 µM) was used as a specific marker of astrocytes following the procedure of Kafitz *et al.*[48]. Astrocytes were also systematically characterized by performing a whole-cell current–voltage profile with a ramp voltage command from −130 to 110 mV (586 ms duration) and also injection of step current to confirm their characteristic passive membrane. Astrocytes with resting membrane potentials more depolarized than −60 mV were rejected. In some experiments, (1,2-bis (o-aminophenoxy)ethane-*N*,*N*,*N*′,*N*′-tetraacetic acid (BAPTA) tetrapotassium salt, 0.1 or 10–35 mM) was added to the internal solution and KCH_3SO_4 or potassium gluconate concentration was adjusted accordingly to maintain potassium ion concentration.

Voltage-clamp experiments. Whole-cell voltage clamp recordings were conducted in presence of several blockers to assess the effects Ca^{2+}, extracellular BAPTA and S100β on pharmacologically isolated Na^+ currents. The modified aCSF used contained (in mM) 131 NaCl, 10 HEPES, 3 KCl, 10 glucose, 2 $CaCl_2$, 2 $MgCl_2$, 10 tetraethylammonium chloride, 10 CsCl, 1 4-aminopyridine and 0.3 $CdCl_2$. The electrodes were filled with a solution containing (in mM) 130 CsF, 9 NaCl, 10 HEPES, 10 EGTA, 1 $MgCl_2$, 3 K_2-ATP, and 1 Na-GTP. The pH and the osmolality were adjusted to 7.2–7.3 and 280–290 mosmol/kg respectively. All current traces were leak subtracted and I_{NaP} current was revealed by subtraction of the currents remaining in riluzole or TTX.

Calcium-sensitive electrodes. Electrodes were made of borosilicate glass pretreated with dimethylchlorosilane and dried at 120 °C for 2 h. The tip of the pipette was filled with calcium ionophore I cocktail A (Sigma-Aldrich, St. Louis, Missouri, USA). The rest of the electrode was filled with $CaCl_2$ (2 M). Before recordings, the electrode was calibrated with aCSF solutions containing increasing concentrations of calcium (0, 0.4, 0.8, 1.2, 1.6 and 2 mM) and the potential jump for each concentration was recorded. The calibration curve obtained from these data was best fitted with a logarithmic function. Only electrodes exhibiting a potential jump higher than 20 mV (mean = 26.96 ± 1.82 mV, n = 13) per decade (that is, between concentrations 0.2 and 2 mM) were kept for our experiments.

Ca^{2+} imaging. Confocal imaging was performed using an Olympus FluoView FV 1000 confocal microscope equipped with a 40× water-immersion lens (Olympus, 0.80 N.A.). The 559-nm diode laser line was used to excite SR101 and the emitted fluorescence was detected through a band-pass filter (570–640 nm). Ca^{2+} indicators (fluo-4, fluo4-AM or fluo8L-AM) and Alexa Fluor 488 were excited with an argon laser line (488 nm) and emission was detected through a band-pass filter (500–545 nm). For Ca^{2+} imaging in single cells, the Ca^{2+} indicator fluo-4 (100 µM, Invitrogen, Grand Island, NY, USA) was added to the internal solution of the recorded cell, while for Ca^{2+} imaging in a population of cells, the slices were incubated for 45–60 min with the cell-permeant Ca^{2+} indicators fluo4-AM (20 µM, Invitrogen, Grand Island, NY, USA) or fluo8L-AM (20 µM, AAT Bioquest, Inc, Sunnyvale, CA, USA) and 0.5% dimethylsulfoxide at room temperature in oxygenated aCSF. Slices were allowed to rest for 30 min before sequence acquisition. Images were acquired at 0.429 s per frame. Offline analysis of sequences was performed with ImageJ software (NIH, USA). Fluorescence intensity was determined on each individual cell by measuring the average pixel values in defined regions of interest (ROIs) on each frame of the sequence. ROIs were placed either on the somata (for AM loading) or on the processes (intra-loading experiment). Changes in fluorescence (ΔF), are presented as relative changes in fluorescence intensity from baseline and expressed as $(\%\Delta F/F_0) = [(F - F_0)/F_0] \times 100$, F_0 being the fluorescence baseline. Because responses were collected over extended periods of time and after repeated NMDA applications, only robust changes of more than 25% were included in the analysis.

Drugs. The following drugs were locally applied near the recorded cells using positive pressure pulses (Picospritzer III) to one or two pipettes: *N*-methyl-D-aspartate (NMDA, 1–2 mM), BAPTA tetrasodium salt (10 mM), glutamate (1 mM). In some experiments, MK-801 (2 mM) and BAPTA tetrapotassium salt (0.1, 10–35 mM) were added to the internal solution of the recording electrode. The following drugs were bath applied: tetrodotoxin (TTX, 1–2 µM), riluzole (20 µM), suramine (50 µM), CNQX (10 µM), cadmium (100 µM), and L-*trans*-pyrollidine-2,4-dicarboxylic acid (PDC) (50 µM). Compounds were purchased from Sigma-Aldrich (Oakville, Ontario, Canada), Tocris Bioscience (Ellisville, Missouri, USA) and Invitrogen (Grand Island, New York, USA).

Antibodies used to pretreat the tissue in some experiments were applied with a large-tip pipette that was lowered to the surface of the tissue near the neuronal and ion-sensitive recording electrodes. The antibody containing pipette was left there to leak for 10–15 min before testing the effects of the antibody. Sometimes a small pressure was applied to eject the antibody from the pipette. Two antibodies were tested: anti-S100β antibody (40 µg/ml, sodium azide salt (140 µM); Sigma-Aldrich, S2532) or nonspecific donkey anti-sheep antibody (120 µg/ml, sodium azide salt (312 µM); Invitrogen–Molecular Probes, A11015).

S100β was synthesized at the Recombinant Proteins and Antibodies Facility of the Institute for Research in Immunology and Cancer of the University of Montreal. A cDNA corresponding to mouse S100β (*S100b*) was subcloned in a pETM14 expression vector harboring an N-terminal hexahistidine tag and a prescission cleavage site. The resulting vector was used to transform BL21 *E. coli* cells for protein expression in Terrific Broth medium supplemented with 1% glucose and 50 μg/ml kanamycin. Cells were grown at 37 °C with vigorous shaking. When the culture reached an OD_{600} of 0.8, the temperature was reduced to 18 °C and expression was induced with 0.5 mM IPTG for 16 h. Cells were then harvested by centrifugation and resuspended in lysis buffer (Tris-HCl 50 mM, pH 8, NaCl 500 mM, BME 5 mM, PMSF 1 mM and one tablet per 100 ml of complete EDTA-free protease inhibitors (Roche Diagnostics). After two cycles of freeze-thaw, cells were sonicated and centrifuged for 1 h at 45,000*g*. Recombinant protein in the supernatant was purified by metal affinity chromatography on a POROS-MC20 perfusion chromatography column (with Ni^{2+} as the chelating metal), pre-equilibrated in Tris-HCl 50 mM, pH 8, NaCl 500 mM, BME 5 mM, PMSF 1 mM and EDTA-free protease inhibitor tablet. After extensive washing of the column, bound proteins were eluted with a gradient of imidazole (0–500 mM) in Tris-HCl, 50 mM, pH 8, and NaCl 150 mM. Fractions were analyzed by SDS-PAGE, and positive ones were pooled and further purified on a preparative-scale high-resolution Superdex-200 gel filtration column equilibrated in HEPES, 20 mM, pH 7.4, NaCl 150 mM, BME 5 mM and protease inhibitors. Fractions containing recombinant S100β were pooled and concentrated by ultrafiltration on Amicon Ultra YM-30 membranes to a concentration of 14.0 mg/ml, supplemented with glycerol to a final concentration of 50%, aliquoted and flash frozen in liquid nitrogen before storing at −80 °C. Before use, aliquots of the protein were thawed and microdialyzed overnight using a dialysis device to eliminate the glycerol (Float-A-Lyzer, Spectra/Por) floating in a 20 mM HEPES buffer containing 140 mM of NaCl at pH 7.4. The protein was then reconcentrated using centrifugal filter units (Amicon Ultra). The same buffer (20 mM HEPES containing 140 mM NaCl but no Ca^{2+}) was used to suspend S100β and adjust S100β concentration to either 129 μM for local application in the submerged chamber or 50 μM for local application in the interface chamber. In a second set of experiments, 1.6 mM $CaCl_2$ was added to the buffer used to suspend S100β and the protein was tested at two concentrations in this buffer (129 μM and 1 mM).

The mutated S100β protein was obtained from D. Weber from the Center for Biomolecular Therapeutics, University of Maryland School of Medicine. It was synthesized using similar methods as above, but had two mutated residues, E31A and E72A, in both the pseudo- and typical EF-hand domains. This mutated protein was characterized using nuclear magnetic resonance (NMR), stopped-flow kinetics and thermodynamic binding methods (isothermal titration calorimetry) and shown to have very weak, if any, binding to Ca^{2+}, even at concentrations greater than 20 mM (ref. 25). The mutated protein was also suspended in a 20 mM HEPES buffer containing 140 mM NaCl and 1.6 mM $CaCl_2$, and locally applied at a concentration of 1 mM.

Isothermal titration calorimetry. The apparent dissociation constant (K_d) for calcium binding to recombinant S100β and the effect of anti-S100β monoclonal antibody on calcium binding of S100β was measured by isothermal titration calorimetry (ITC) at 20 °C using a Microcal ITC-200 microcalorimeter (GE Healthcare). The recombinant protein was dialyzed extensively against 20 mM HEPES, pH 7.4, containing 20 mM NaCl, and $CaCl_2$ was added to 2 mM in the resulting dialysis buffer. S100β at a concentration of 25 μM in the reservoir was titrated with 16 injections of 2.5 μl of the 2 mM $CaCl_2$ solution. To verify the effect of antibody binding on S100β calcium binding capacity, a preformed complex of 25 μM S100β and 50 μM monoclonal S100β antibody was dialyzed against the same buffer and titrated with 2 mM $CaCl_2$. The resulting thermograms for both experiments were analyzed with the ORIGIN 7 software.

Analysis of firing patterns. Firing patterns were characterized as tonic or rhythmic bursting discharge. Tonic discharge typically consisted of low-frequency single spikes separated by regular but relatively long intervals (interspike intervals: ISI of 150–300 ms; **Supplementary Fig. 1**). In intracellular recordings these intervals appeared as afterhyperpolarizations. In transition between tonic and burst firing, the afterhyperpolarization gradually reverted into an afterdepolarization which often gave rise to a second spike (**Supplementary Fig. 1**, middle panel) at a very short ISI. Although these doublets resembled burst firing, we used more stringent criteria for the latter by defining bursts as clusters of at least three action potentials occurring at high frequency (>130 Hz) followed by a long silent period. In intracellular records, bursts appeared as depolarizing plateaus over-ridden by at least three actions potentials. The period separating the beginning of two consecutive plateaus was used to calculate the inter-burst frequency in intracellular recordings, whereas in extracellular recordings, the period separating the first spike of two consecutive bursts was used for this measure. Bursting frequency was calculated only in neurons that displayed a stable rhythmic discharge for more than five cycles. In both types of recording, the ISI of action potentials within a burst was used to calculate the intra-burst frequency.

Immunohistochemistry. Standard immunocytochemical procedures as reported in Panatier *et al.* (2011)[34] were used for immunostainings of S100β in NVsnpr.

Statistics. Data are presented as mean ± s.e.m. throughout the text. No statistical methods were used to predetermine sample sizes, but our sample sizes are similar to those generally employed in the field. Since there was no a priori treatment of the animals, no procedures were used for blinding or randomization. Parametric tests were used when data was distributed normally according to the Kolmogorov-Smirnov test. In that case, between groups comparisons were performed with ANOVAs and, for pairwise comparisons, paired *t*-tests, independent *t*-tests or Tukey's tests were used. Otherwise, non-parametric tests were used. Groups were compared with Kruskal-Wallis and Dunn's post test for multiple comparisons, while Mann-Whitney test was used for pairwise comparisons. Probabilities of α-type errors of <0.05 were considered to be significant.

A **Supplementary Methods Checklist** is available.

48. Kafitz, K.W., Meier, S.D., Stephan, J. & Rose, C.R. Developmental profile and properties of sulforhodamine 101–labeled glial cells in acute brain slices of rat hippocampus. *J. Neurosci. Methods* **169**, 84–92 (2008).

doi:10.1038/nn.4013